THE JOURNAL OF BIOLOGICAL CHEMISTRY VOL. 287, NO. 52, pp. 43899–43908, December 21, 2012

Structural Basis of Molecular Recognition between ESCRT-III-like Protein Vps60 and AAA-ATPase Regulator Vta1 in the Multivesicular Body Pathway*[S]◆

Received for publication, June 25, 2012, and in revised form, October 19, 2012 Published, JBC Papers in Press, October 26, 2012, DOI 10.1074/jbc.M112.390724

Zhongzheng Yang[‡], Cody Vild[§], Jiaying Ju[‡], Xu Zhang[¶], Jianping Liu[‡‖], Jie Shen[‡], Bin Zhao[‡], Wenxian Lan[‡], Fuchun Gong[‖], Maili Liu[¶], Chunyang Cao[‡1], and Zhaohui Xu[§2]

From the [‡]State Key Laboratory of Bioorganic and Natural Products Chemistry, Shanghai Institute of Organic Chemistry, Chinese Academy of Sciences, Shanghai 200032, China, the [§]Life Sciences Institute and Department of Biological Chemistry, Medical School, University of Michigan, Ann Arbor, Michigan 48109, the [¶]State Key Laboratory of Magnetic Resonance and Atomic and Molecular Physics, Wuhan Institute of Physics and Mathematics, Chinese Academy of Sciences, Wuhan 430071, China, and the [‖]Institute of Chemistry and Biochemical Engineering, Changsha University of Science and Technology, Changsha 410076, China

Background: Vps4 ATPase is stimulated by the interaction between Vta1 and Vps60, but the structural basis for this interaction remains unclear.
Results: The structure of the Vta1 N-terminal domain (Vta1NTD) in complex with Vps60(128–186) was determined.
Conclusion: Vps60(128–186) interacts with Vta1NTD through helices α4′ and α5′, extending over Vta1NTD MIT2 domain helices 1–3.
Significance: This is a novel MIT recognition mode.

The AAA-ATPase Vps4 is critical for function of the multivesicular body sorting pathway, which impacts cellular phenomena ranging from receptor down-regulation to viral budding to cytokinesis. Vps4 activity is stimulated by the interaction between Vta1 and Vps60, but the structural basis for this interaction is unclear. The fragment Vps60(128–186) was reported to display the full activity of Vps60. Vta1 interacts with Vps60 using its N-terminal domain (Vta1NTD). In this work, the structure of Vps60(128–186) in complex with Vta1NTD was determined using NMR techniques, demonstrating a novel recognition mode of the microtubule-interacting and transport (MIT) domain in which Vps60(128–186) interacts with Vta1NTD through helices α4′ and α5′, extending over Vta1NTD MIT2 domain helices 1–3. The Vps60 binding does not result in Vta1 conformational changes, further revealing the fact that Vps4 ATPase is enhanced by the interaction between Vta1 and Vps60 in an unanticipated manner.

Membrane budding away from the cytosol controls a number of biological processes important to cellular homeostasis and defenses against aging (1–3). The machinery responsible for executing this function consists of several distinct multimeric complexes known as the endosomal sorting complexes required for transport (ESCRTs)[3] (4–6), which were originally identified in yeast and have been implicated in multivesicular body (MVB) biogenesis in plants, fungi, and animals (6, 7). MVBs are formed when the late endosomal membrane invaginates and forms vesicles in the lumen, carrying selected transmembrane protein cargoes in the budding process (2, 3). MVB biogenesis and fusion of an MVB with the lysosome in a later step represent a mechanism in which eukaryotic cells down-regulate cell surface signaling via the endolysosomal degradation pathway (8). Components of the ESCRT machinery have been identified as potential tumor suppressors (9), mainly attributed to the involvement of the ESCRT machinery in mediating signal attenuation for activated receptors of growth factors, peptide hormones, and cytokines. The ESCRT machinery protects against age-related neurodegenerative diseases through either the canonical MVB pathway or autophagy (9, 10). In addition, the ESCRT machinery also plays a pathological role in viral infection (2, 11, 12).

At least five distinctive multimeric complexes are involved in MVB biogenesis: ESCRT-0, ESCRT-I, ESCRT-II, ESCRT-III, and Vps4 (13, 14). Their structure and function are highly conserved in all eukaryotes (9, 10). ESCRT-0 is responsible for clustering of ubiquitylated cargoes to the site of MVB formation. ESCRT-I and ESCRT-II together generate membrane curva-

* This work was supported by National Basic Research Program of China Grants 2009CB918600 and 2011CB966300, National Science Foundation of China Grants 30970595 and 20921091, International Cooperation Foundation Grant 09540703800 from the Science and Technology Commission of Shanghai Municipality, National New Drug Design Program Grant 2011ZX09506 from the Ministry of Health of China, and Grant T151102 from the State Key Laboratory of Magnetic Resonance and Atomic and Molecular Physics, Wuhan Center for Magnetic Resonance, Wuhan Institute of Physics and Mathematics, Chinese Academy of Sciences.
◆ This article was selected as a Paper of the Week.
[S] This article contains supplemental Figs. S1 and S2.
[1] To whom correspondence may be addressed: State Key Laboratory of Bioorganic and Natural Products Chemistry, Shanghai Institute of Organic Chemistry, Chinese Academy of Sciences, 345 Lingling Rd., Shanghai 200032, China. Tel.: 86-21-5492-5491; Fax: 86-21-6416-6128; E-mail: ccao@mail.sioc.ac.cn.
[2] To whom correspondence may be addressed. Tel.: 734-615-2077; Fax: 734-763-6492; E-mail: zhaohui@umich.edu.

[3] The abbreviations used are: ESCRT, endosomal sorting complex required for transport; MVB, multivesicular body; MIT, microtubule-interacting and transport; MIM, MIT-interacting motif; Vta1NTD, Vta1 N-terminal domain; SUMO, small ubiquitin-like modifier; HSQC, heteronuclear single-quantum correlation.

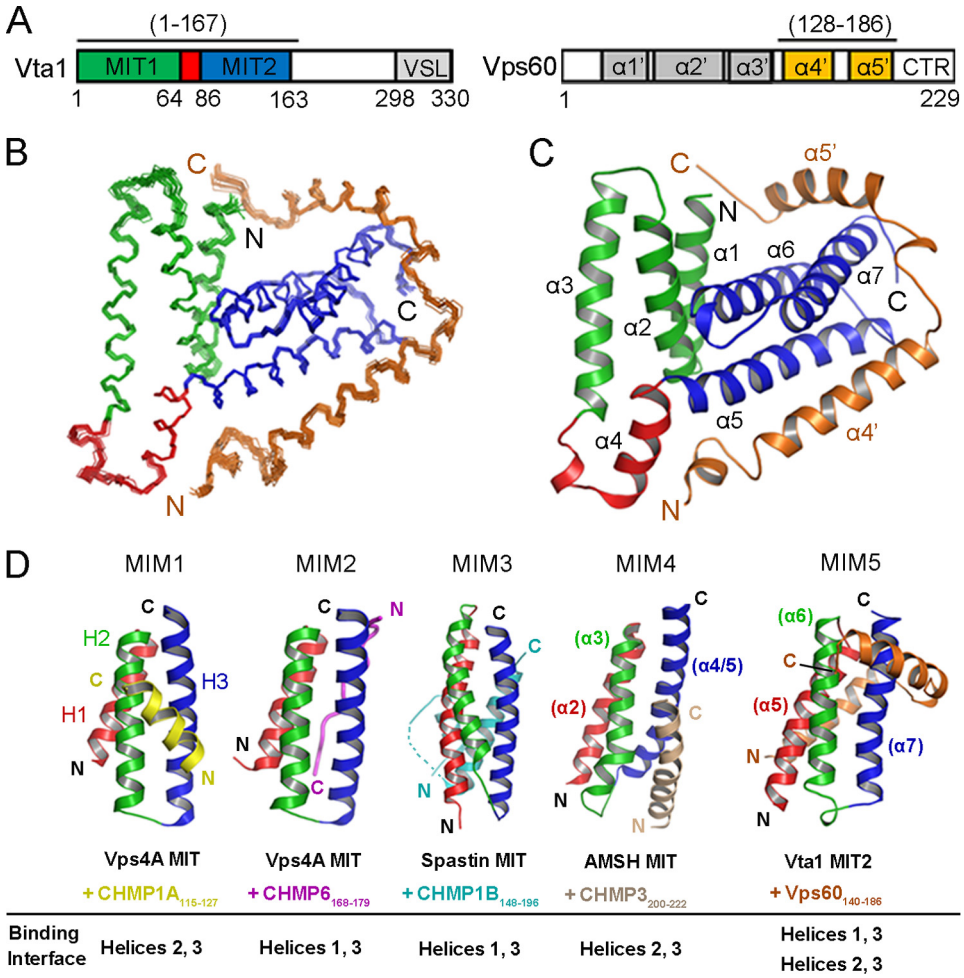

FIGURE 1. **Structural feature of the Vta1NTD-Vps60(128–186) complex.** *A*, schematic representation of Vta1 and Vps60, highlighting regions critical for interactions that contribute to increased Vps4 ATPase activity. VSL, Vta1/SBP1/LIP5; CTR, C-terminal region. *B*, backbone view of the ensemble of the 20 lowest energy Vta1NTD-Vps60(128–186) NMR structures, where Vps60(128–186) is displayed in *orange*. *C*, three-dimensional representative structure of Vta1NTD-Vps60(128–186). The helices are numbered. *D*, structural comparison of five different recognition modes of the MIT domain with MIM. Vps60 interacts with the first, second, and third helices of the Vta1NTD MIT2 domain together, which is different from a previously reported MIT ligand recognition mode.

ture and budding, whereas assembly of ESCRT-III at the bud neck catalyzes scission of the membrane. Completion of the process requires the AAA-ATPase Vps4, which disassembles ESCRT-III polymers upon ATP binding and hydrolysis (15, 16). This ATP-consuming reaction is the only step in MVB biogenesis that inputs energy into the system, therefore providing the thermodynamic driving force for processing. Importantly, the role of Vps4 is conserved in all biological processes that depend on the action of the ESCRTs. Similar to other AAA-ATPases, Vps4 functions as an oligomer whose structure likely contains two conformationally distinctive hexameric rings (17). The rings contain a central pore where ESCRT-III subunits may physically interact and pass through during the disassembly process. Initial binding of Vps4 to ESCRT-III subunits requires its N-terminal microtubule-interacting and transport (MIT) domain (18). The MIT domain appears to specifically recognize short peptide sequence MIT-interacting motifs (MIMs) at or near the C-terminal end of ESCRT-III subunits (19–24).

The *in vivo* activity of Vps4 is tightly regulated (25). To date, at least four proteins have been identified to bind to Vps4 and have roles in regulating its oligomerization and activity (26–29). Did2, Ist1, and Vps60 are ESCRT-III-related proteins whose mechanisms of action on Vps4 remain to be clarified. Vta1 is a positive regulator of Vps4 by promoting Vps4 oligomerization (26, 30). Structural study of Vta1 has shown that it is a molecular dimer, with each subunit folded into two terminal domains linked by a flexible linker (29). Its C-terminal domain mediates dimerization and binds to a unique β-domain in the Vps4 AAA domain (31, 32). Its N-terminal domain (residues 1–167; Vta1NTD) (Fig. 1) contains two tandem MIT domains, which specifically recognize Vps60 and Did2 but not other ESCRT-III subunits (27, 29). The fragment Vps60(128–186) was reported to display the full activity of Vps60, which stimulates Vps4 ATPase in a Vta1-dependent manner (27).

In this work, to investigate how Vps60 interacts with Vta1NTD, we first measured the binding affinity of Vta1NTD for Vps60(128–186) ($K_d \sim 0.7\ \mu$M) using isothermal titration calorimetry assay and then determined the solution structure of Vta1NTD in complex with Vps60(128–186). To confirm the residues involved in the interaction between Vta1NTD and Vps60(128–186), site-directed mutations and GST pulldown experiments were performed. The structure reveals that

Vps60(128–186) interacts with Vta1NTD through a novel MIT domain recognition mode distinct from any reported mechanism.

EXPERIMENTAL PROCEDURES

Cloning, Expression, and Purification—DNA fragments encoding yeast Vta1 and Vps60 were amplified from *Saccharomyces cerevisiae* genomic DNA. Vta1NTD or Vps60(128–186) was expressed in *Escherichia coli* BL21(DE3) using a modified pET28b vector with a small ubiquitin-like modifier (SUMO) protein inserted between a His_6 tag and the Vta1NTD or Vps60(128–186) coding region, respectively. His_6-tagged SUMO-Vta1NTD or His_6-tagged SUMO-Vps60(128–186) was purified by nickel-nitrilotriacetic acid affinity chromatography following standard procedures. Ulp1 protease was then added to remove the His_6-SUMO tag, and the protein mixture was passed over a second nickel-nitrilotriacetic acid column and further purified by anion exchange chromatography on a Resource Q column (GE Healthcare). For isotope labeling, M9 minimal medium was supplemented with $^{15}NH_4Cl$ (Cambridge Isotope Laboratories) or $^{15}NH_4Cl$ and 2 g/liter [^{13}C]glucose (Cambridge Isotope Laboratories). Derivative proteins were purified in the same way as native proteins.

NMR Sample Preparation and Data Collection—Differentially labeled complex samples in 25 mM sodium phosphate (pH 7.0), 100 mM NaCl, 5 mM DTT-d_{10}, and 0.02% NaN_3 were prepared as follows: 1) 1.5 mM uniformly labeled $^{15}N/^{13}C$-labeled Vta1NTD plus 1.8 mM unlabeled Vps60(128–186) and 2) 1.5 mM uniformly labeled $^{15}N/^{13}C$-labeled Vps60(128–186) in complex with 1.8 mM unlabeled Vta1NTD. All NMR experiments were performed at 20 °C on a Varian Unity Inova 600 NMR spectrometer (with cryo-probe) equipped with triple resonances and pulsed-field gradients or on a Bruker AVANCE III 800-MHz NMR spectrometer (with cryo-probe) equipped with four channels and *z* axis pulsed-field gradient. The standard suite of experiments for assigning the ^1H, ^{13}C, and ^{15}N backbone and side chain chemical shifts of bound ^{13}C- and ^{15}N-double-labeled Vta1NTD in complex with unlabeled Vps60(128–186) or of bound ^{13}C- and ^{15}N-double-labeled Vps60(128–186) in complex with unlabeled Vta1NTD and for the collection of NOE-based distance restraints were measured (33, 34), including two-dimensional ^{13}C-edited heteronuclear single-quantum correlation (HSQC) in both aliphatic and aromatic regions and ^{15}N-edited HSQC; three-dimensional HNCA, HNCO, HN(CO)CA, HNCACB, CBCA(CO)NH, and ^{15}N-resolved HSQC- and HCCH-total correlation spectroscopy in both aliphatic and aromatic regions; ^{15}N-resolved and ^{13}C-resolved HSQC-NOESY for both aliphatic and aromatic resonances; and two-dimensional (Hβ)Cβ(CγCδ)Hδ and (Hβ)Cβ(CγCδCϵ)Hϵ spectra for correlation of Cβ and Hδ or Hϵ in aromatic rings used in aromatic proton assignment (35). The intermolecular NOEs between labeled Vta1NTD or the Vps60(128–186) peptide and the unlabeled Vps60(128–186) peptide or Vta1NTD were obtained by analyzing three-dimensional ^{13}C-F1-edited, $^{13}C/^{15}N$-F3-filtered NOESY spectra, respectively. All spectra were processed with the program NMRPipe (36) and analyzed with the SPARKY 3 software (37). The ^1H chemical shifts were referenced to 2,2-dimethylsilapentane-5-sulfonic acid, and the ^{13}C and ^{15}N resonances were indirectly referenced to 2,2-dimethylsilapentane-5-sulfonic acid.

NMR Structure Calculation—Calculations were carried out using a standard simulated annealing protocol implemented in the program XPLOR-NIH 2.19. Interproton distance restraints derived from NOE intensities were grouped into three distance ranges, 1.8–2.9, 1.8–3.5, and 1.8–6.0 Å, corresponding to strong, medium, and weak NOEs, respectively. The dihedral angles ϕ and ψ were derived from the backbone chemical shifts (HN, HA, CO, and CA) using the program TALOS (36, 38). Slowly exchanging amide protons, identified in the two-dimensional ^{15}N HSQC spectra recorded after a H_2O buffer was exchanged with a D_2O buffer, were used in the structure calculated with the NOE distance restraints to generate hydrogen bonds for the final structure calculation, as done in the literature (39). A total of 10 iterations (50 structures in the initial eight iterations) were performed. 100 structures were computed in the last two iterations; 20 conformers with the lowest energy were used to represent the three-dimensional structures. In the ensemble of the simulated annealing 20 structures, there was no distance constraint violation of $>$0.3 Å and no torsion angle violation of $>3°$. The final 20 structures with the lowest energy were evaluated with the programs PROCHECK-NMR and PROCHECK (40) and are summarized in Table 1. All figures were generated using the programs PyMOL and MOLMOL (41).

Isothermal Titration Calorimetry—To obtain a direct binding affinity between Vta1NTD (wild-type and mutants) and the Vps60(128–186) peptide, wild-type Vta1NTD and mutants were titrated with the Vps60(128–186) peptide using an iTC-200 microcalorimeter (GE Healthcare) at 25 °C. All proteins and peptides were exchanged with buffer containing 20 mM sodium phosphate(pH 7.0) and 0.1 M NaCl by gel filtration chromatography, centrifuged to remove any particulates, and degassed. To obtain a direct binding affinity between Vta1NTD variants and the Vps60(128–186) peptide, a solution of ~0.1 mM wild-type and mutant Vta1NTD was titrated with 1.0 mM Vps60(128–186) peptide, respectively. The accurate concentrations of Vta1NTD and its mutants were determined using their A_{280} constants.

Circular Dichroism Spectroscopy of Free Vps60(128–186)—To probe the folding of free Vps60(128–186), the CD experiment was performed at 25 °C on a JASCO-715 spectropolarimeter (Jasco International Co., Tokyo, Japan). Data were collected at 0.1-nm intervals at a scan speed of 20 nm/min, 1-nm bandwidth, and 0.25-s response time from 250 to 190 nm. Circular quartz cells of 1- and 0.1-cm path length were used for the far-UV regions. The CD intensities are expressed as molar residue ellipticities given in units of degrees $cm^2\ mol^{-1}$. The concentration of Vps60(128–186) was ~10 μM. The buffer conditions used for running CD spectra were 20 mM sodium phosphate and 50 mM NaCl (pH 7.5).

GST Pulldown Experiments—The experiments were performed following standard procedures in buffer containing 25 mM Tris-HCl (pH 8.0), 150 mM NaCl, and 5 mM 2-mercaptoethanol. Purified wild-type Vta1NTD and mutants were incubated with GST alone or with GST-tagged Vps60(128–186) immobilized on glutathione-agarose beads for 3 h at 4 °C. The

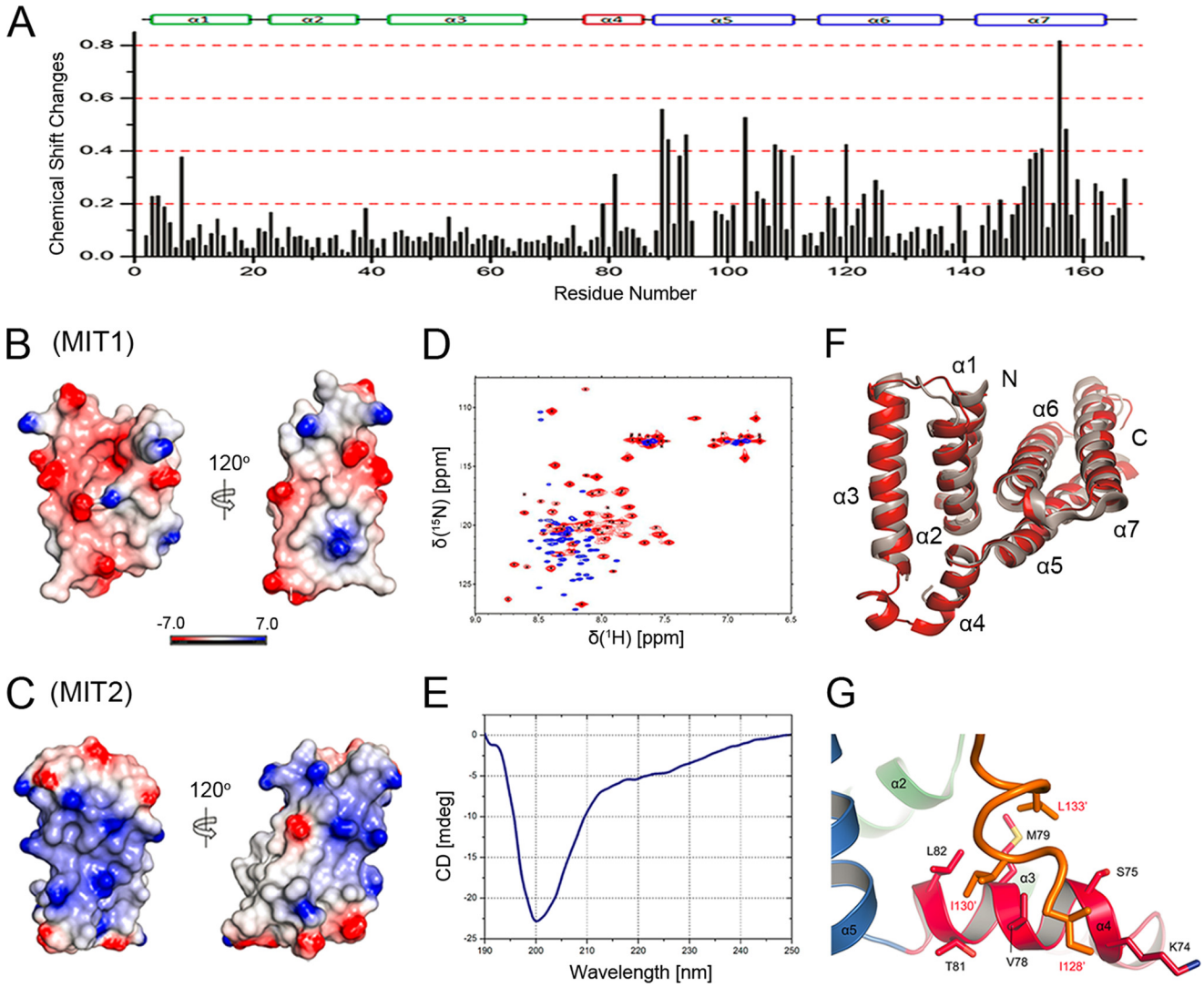

FIGURE 2. **Vps60 interacts with the Vta1NTD MIT2 domain motif, resulting in conformation stabilization of Vps60 and Vta1NTD helix α4.** *A*, chemical shift changes in Vta1NTD backbone amide atoms ^{1}H and ^{15}N upon Vps60(128–186) binding, calculated using the following equation: $\Delta\delta_{av} = (0.5 \times (\Delta\delta(NH)^2 + 0.2 \times \Delta\delta(^{15}N)^2))^{1/2}$. The secondary structures are indicated at the top based on the crystal structure of free Vta1NTD (Protein Data Bank code 2RKK). *B* and *C*, electrostatic potential surfaces between helices 1 and 3 (*left*), helices 2 and 3 (*right*) of the MIT1 domain and between helices 1 and 3 (*left*) and helices 2 and 3 (*right*) of the MIT2 domain, respectively. The electrostatic potential surface was generated based on the crystal structure of free Vta1NTD using DelPhi software and visualized by PyMOL. *D*, superimposition of two-dimensional ^{1}H-^{15}N HSQC spectra of Vps60(128–186) in the absence (*blue*) and presence (*red*) of Vta1NTD. *E*, CD spectroscopy of free Vps60(128–186). *F*, structural overlay of Vta1NTD in the free state (*gray*) and in complex with Vps60(128–186) (*red*). The N and C termini and the secondary structures are indicated. *G*, interactions between the short N-terminal α-helix of Vps60(128–186) and helix α4 of Vta1NTD. The ribbon representation of Vta1NTD is colored in *green* for α2 and α3, *red* for α4, and *blue* for α5, with the N-terminal α-helix of Vps60(128–186) shown in *orange*.

beads were then washed extensively three times with the above buffer, and bound proteins were separated by SDS-PAGE and visualized by Coomassie Blue staining.

RESULTS

NMR Structural Determination—Initially, two basic sets of NMR mixed samples were made: 1) ^{13}C and ^{15}N isotope-labeled Vta1NTD with unlabeled Vps60(128–186) at a stoichiometric ratio of 1:1.2 and 2) ^{13}C and ^{15}N isotope-labeled Vps60(128–186) with unlabeled Vta1NTD at a stoichiometric ratio of 1:1.2, each of them for assignment of NMR signals belonging to the corresponding ^{13}C- and ^{15}N-labeled component and its structural determination. The intermolecular NOEs could be correctly assigned by confirming signals observed in three-dimensional ^{13}C-F1-edited, $^{13}C/^{15}N$-F3-filtered NOESY spectra acquired on both complex samples. In total, assignments of >96% of the main chain and 95% of the side chain atoms of the residues in the complex were completed. The NMR chemical shift changes of Vta1NTD backbone atoms ^{1}H and ^{15}N in the absence and presence of Vps60(128–186) reveal that Vps60(128–186) addition mainly induced Vta1NTD MIT2 domain amide ^{15}N and ^{1}H chemical shift variations in residues of the Vta1NTD MIT2 domain (Fig. 2*A*), suggesting that Vps60-binding sites localize in these regions. This observation accords with the analysis of the electrostatic surface of Vta1NTD in its free state, which shows that the Vta1NTD MIT2 domain is more positively charged than the MIT1 domain (Fig. 2, *B* and *C*), suitable for negatively charged Vps60 binding.

The solution structure of the Vta1NTD-Vps60(128–186) complex was determined by a conventional heteronuclear NMR method using ^{15}N- or $^{13}C/^{15}N$-labeled protein. In total,

TABLE 1
Experimental restraints and structural statistics for the Vta1NTD-Vps60(128–186) complex

NMR distance and dihedral constraints	
Distance restraints from NOEs	
Intramolecular	
Total	4183
Intraresidue ($i - j = 0$)	1215
Sequential ($\|i - j\| = 1$)	971
Medium-range ($1 < \|i - j\| \leq 5$)	1340
Long-range ($\|i - j\| > 5$)	657
Intermolecular	286
Hydrogen bonds	260
Dihedral restraints	390
φ	195
ψ	195
Structural statistics[a]	
r.m.s.d.[b] *versus* mean structure (Å)	
All backbone atoms	0.59 ± 0.13
All heavy atoms	1.07 ± 0.15
Backbone atoms (secondary structure)	0.46 ± 0.10
Heavy atoms (secondary structure)	0.87 ± 0.12
r.m.s.d. from experimental restraints	
NOE distances (Å)	0.023 ± 0.0003
Dihedral angles	0.685 ± 0.0136°
r.m.s.d. deviations from idealized geometry	
Bonds (Å)	0.0018 ± 0.000021
Angles	0.280 ± 0.0038°
Impropers	0.289 ± 0.0039°
Ramachandran analysis (%)	
Residues in most favored regions	94.1
Residues in additionally allowed regions	4.8
Residues in generously allowed regions	1.1
Residues in disallowed regions	0.0

[a] Structural statistics were calculated from the 20 lowest energy XPLOR-NIH structures.
[b] r.m.s.d., root mean square deviations.

4469 distance restraints from NOE (286 intermolecular NOEs), 260 hydrogen bonds, and 390 dihedral angle restraints for backbone φ and ψ angles were used to calculate the solution structure. A best fit superposition of the ensemble of the 20 lowest energy structures represented in Fig. 1*B* is displayed, with root mean square deviations of 0.59 ± 0.13 Å for global backbone atoms and 1.07 ± 0.15 Å for global heavy atoms. The root mean square deviations were 0.46 ± 0.10 Å for the backbone atoms (N, Cα, and CO) and 0.87 ± 0.12 Å for all heavy atoms in the well ordered secondary structure regions. The Ramachandran plot displays 94.1% of the residues in the most favored regions and 4.8% residues in additionally allowed regions (Table 1), indicating that the structures are reasonable.

Vta1 Binding Stabilizes Vps60(128–186) Helix Conformation—The two-dimensional NMR ^{1}H-^{15}N HSQC experiment with Vps60(128–186) in its free state (Fig. 2*D*) suggests that Vps60(128–186) in its free state is disordered because the cross-peaks are not dispersed, localizing mainly in the region between 8.0 and 8.5 ppm. To confirm this observation, we preformed CD spectroscopy on free Vps60(128–186), where negative absorption at ~200 nm shows a random coil conformation (Fig. 2*E*). Upon binding to Vta1NTD, the cross-peaks in two-dimensional NMR ^{1}H-^{15}N HSQC of Vps60(128–186) became dispersed (Fig. 2*D*), suggesting that Vps60(128–186) folds into an ordered structure, coinciding with the structure determined below. This demonstrates that Vta1NTD binding stabilizes Vps60 helix conformation.

Overall Complex Structure—The Vta1NTD-Vps60(128–186) structure shows that the bound Vta1NTD still has two MIT domains, each of them composed of three α-helices (MIT1: helices α1, α2 and α3; and MIT2: helices α5, α6, and α7) (Fig. 1*C*), almost similar to those observed in its free state (29). Helix α4 was much longer in Vta1NTD bound to Vps60(128–186) than in free Vta1NTD, which might have resulted from the conformational stabilization upon its binding to Vps60 (as demonstrated below), consistent with the secondary structure prediction based on the assignments of backbone atoms ^{13}Cα, ^{13}Cβ, ^{13}CO, ^{1}H, and ^{15}N (supplemental Fig. S1). The backbone atoms of bound Vta1NTD had a root mean square deviation of 1.07 Å from those of free Vta1NTD (Fig. 2*F*), indicating that Vps60(128–186) binding does not induce overall major conformational changes in Vta1NTD. The secondary structure prediction and perceived structural homology to ESCRT-III protein Vps24/CHMP3 suggest that Vps60(128–186) corresponds to the fourth and the fifth helices within the Vps60 structure (42). In the current complex structure, Vps60(128–186) indeed folds into two α-helices (denoted as α4′ and α5′), and both helices are involved in the interaction with the MIT2 domain of Vta1NTD (Fig. 1). The two α-helices of bound Vps60(128–186) adopt an overall V-shaped helix-turn-helix structure and straddle on the third helix (α7) of the Vta1NTD MIT2 domain. The longer helix α4′ consists of residues 140′–157′ and interacts with α5 and α7, corresponding to the first and third helices of the Vta1NTD MIT2 domain. It runs diagonally from the N-terminal end of α5 to the C-terminal end of α7, maintaining a general direction parallel to both helices. The polypeptide chain crosses over to the other side of α7 near the C-terminal end of α7 and continues as α5′ (residues 168′–182′), running nearly vertical to helices α6 and α7. The Vta1-Vps60 complex buries a total of ~3600-Å^2 surface area at the interface. In contrast to the MIT domains in Vps4, spastin, or AMSH (19–24), Vps60(128–186) interacts with Vta1NTD through helices α4′ and α5′, extending over Vta1NTD MIT2 domain helices 1–3. Thus, the Vta1NTD MIT2 domain displays a fifth and novel ligand recognition mode to bind to Vps60(128–186) (Fig. 1*D* and shown under "Discussion").

Vta1NTD Helix 4 Is Stabilized upon Vps60 Binding—In our complex structure, there are no significant structural changes in Vta1NTD except in the region that connects the two MIT domains. In the free Vta1NTD structure (29), the linker adopts largely a random coil structure, with only a one-turn α-helix occurring at residues 80–84. In particular, residues 65–75 appear to be disordered in the structure. Upon Vps60 binding, the linker becomes ordered. Residues 68–71 become a one-turn α-helix, and residues 73–84 adopt a longer helical structure (Fig. 2*F*). This conformational change might be caused by the interactions between helix α4 (positions 73–84) of Vta1NTD and a short N-terminal α-helix (positions 128–134) of Vps60(128–186) (Fig. 2*G*). The interaction is predominantly hydrophobic, involving Ile-128′, Ile-130′, and Leu-133′ of Vps60, as well as Lys-74, Ser-75, Val-78, Met-79, Thr-81, and Leu-82 of Vta1NTD helix α4.

To confirm that the changes in helix α4 of Vta1NTD are generated due to Vps60(128–186) binding rather than crystallization, we assigned the chemical shifts of backbone atoms ^{13}Cα, ^{13}Cβ, ^{13}CO, ^{1}H, and ^{15}N of free Vta1NTD. The secondary structure prediction based on these assignments using the programs CSI (43) and TALOS (36, 38) suggests that there are

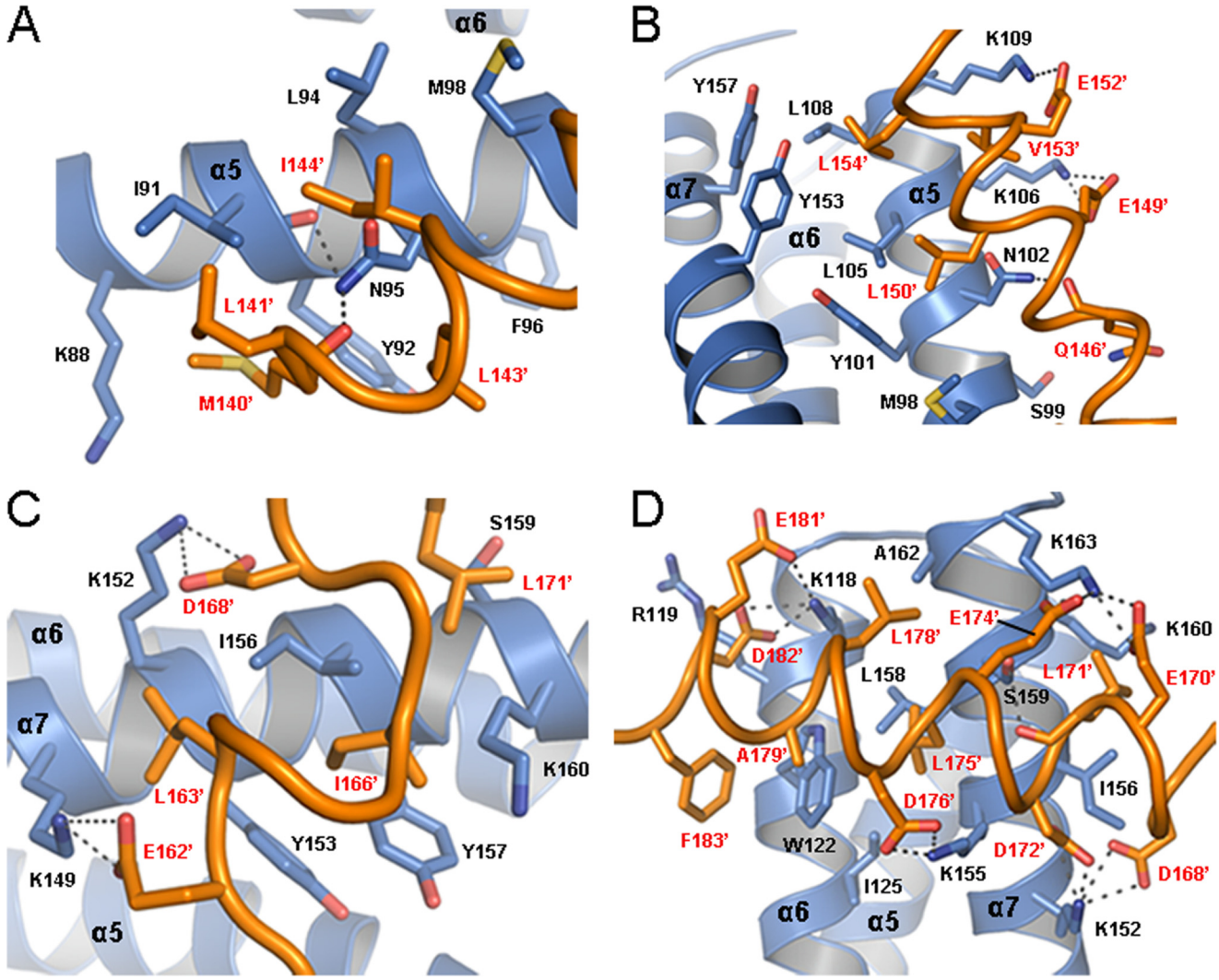

FIGURE 3. **Detailed interactions between Vps60(128–186) and the Vta1NTD MIT2 domain.** *A* and *B*, ribbon representation of Vta1NTD shown in *blue*, with Vps60(128–186) helix α4′ shown in *orange*. *C*, ribbon representation of Vta1NTD shown in *blue*, with the linker between Vps60(128–186) helices α4′ and α5′ shown in *orange*. *D*, ribbon representation of Vta1NTD shown in *blue*, with Vps60(128–186) helix α5′ shown in *orange*.

seven helices formed in free Vta1NTD, including α1 (Ala-2–Lys-17), α2 (Ile-23–Leu-36), α3, (Gln-43–Glu-62), α4 (Asp-73–Met-79), α5 (Gln-86–Lys-109), α6 (Val-115–Leu-134), and α7 (Thr-142–Lys-163), which are much similar to these observed in Vta1NTD bound to Vps60(128–186), except helix α4 (supplemental Fig. S1).

Interface in the Vta1-Vps60 Complex Structure—There are three major sites of interaction between the Vta1NTD MIT2 domain and Vps60(128–186) (Fig. 3). The first binding site (Fig. 3, *A* and *B*) on Vta1NTD is predominantly hydrophobic and is lined by Ile-91, Tyr-92, Leu-94, Phe-96, Met-98, Tyr-101, Leu-105, Leu-108, Tyr-153, and Tyr-157 and the aliphatic chain of Lys-88, Lys-106, and Lys-109. The side chains of the residues located at Vps60(128–186) helix α4′, including Met-140′, Leu-141′, Leu-143′, Ile-144′, Leu-150′, Val-153′, and Leu-154′, are inserted into the groove of Vta1NTD helices 5 and 7. The Vps60(128–186) Ile-144′ side chain has a hydrophobic interaction with the Vta1NTD Ile-91, Leu-94, and Met-98 side chains, as Pro-171 functions in the complex Vps4A-CHMP6(168–179) (21). Besides the hydrophobic interactions, complementary salt bridges are also formed by two of the adjacent conserved Vps60(128–186) residues (Glu-149′ and Glu-152′) (Fig. 3*B*). Moreover, the side chains of Vta1NTD Asn-95 and Asn-102 may form hydrogen bond interactions with the main chains of Met-140′ and Gln-146′, respectively. The second site on Vta1NTD binds mainly to the linker between α4′ and α5′ of Vps60(128–186) (Fig. 3*C*), most prominently to the side chains of Leu-163′ and Ile-166′. This site is also mainly hydrophobic and is lined by Tyr-153, Ile-156, and Tyr-157 and the aliphatic chains of Lys-149, Lys-152, and Lys-160, except that the side chain of Glu-162′ forms a complementary salt bridge with Lys-149. A previous alanine-scanning mutagenesis study showed that residues 139′–143′, 144′–148′, 154′–158′, and 164′–168′ of Vps60 are important for its interaction with Vta1 (27), which is consistent with our current structural observation. The third binding site on Vta1 contacts Vps60(128–186) helix α5′ (Fig. 3*D*), including previously identified Vta1 residues important for Vps60 interaction, Trp-122 and Lys-152 (27, 29). In addition, the side chains of polar residues Lys-118, Arg-119, Lys-155, Lys-160, and Lys-163, as well as residues Ile-125, Ile-156,

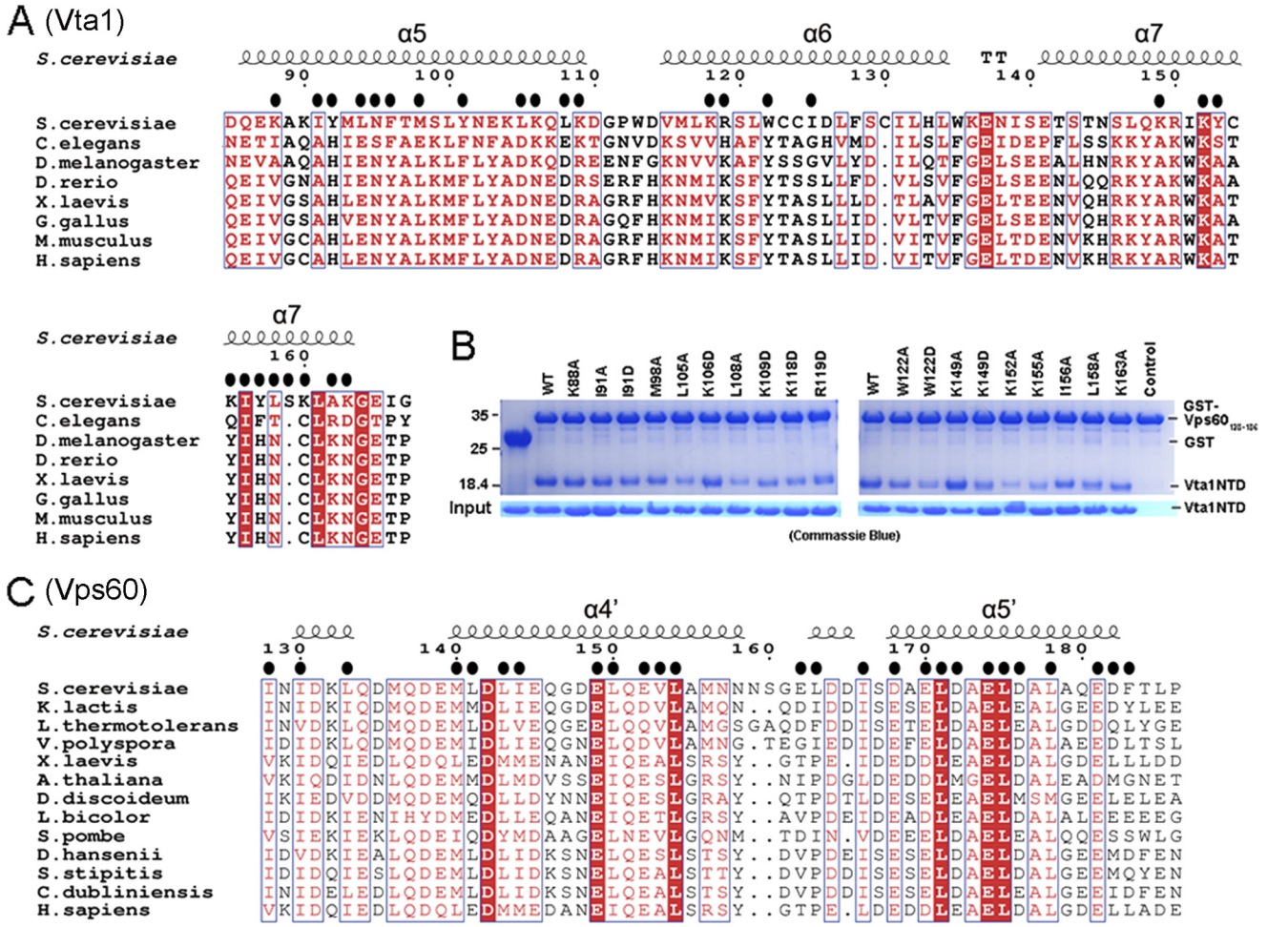

FIGURE 4. **Sequential and mutational analyses of the Vta1NTD-Vps60(128–186) complex.** *A*, structure-based sequence alignments of the Vta1NTD MIT2 domain from various organisms. The residues involved in the interactions are indicated (*black ovals*). *B*, GST pulldown assay of the Vta1NTD-Vps60(128–186) complex. GST or GST-tagged Vps60(128–186) was used to pull down wild-type or mutant Vta1NTD as indicated. Proteins retained on the beads were analyzed by SDS-PAGE and visualized by Coomassie Blue staining. *C*, sequence alignment of Vps60(128–186) helices α4′ and α5′ from various organisms. The residues involved in the interaction are indicated (*black ovals*).

Leu-158, and Ala-162, largely hydrophobic in nature, form salt bridges with those of Asp-168′, Glu-170′, Asp-172′, Glu-174′, Asp-176′, Glu-181′, and Asp-182′ or have hydrophobic or stacking interactions with those of Leu-171′, Leu-175′, Leu-178′, Ala-179′, and F183′. A hydrogen bond interaction was observed between the side chain of Ser-159 and the main chain of Leu-171′.

Mutational Analyses of the Vta1-Vps60 Interaction—Mutations were introduced into these observed binding sites to test the importance of the residues to the overall stability of the complex. As shown in Fig. 4, Table 2, and supplemental Fig. S2, our *in vitro* GST pulldown experiments and isothermal titration calorimetry assay demonstrated that of all the single alanine or aspartic acid substitutions of Vta1NTD Lys-88, Ile-91, Met-98, Leu-105, Lys-106, Leu-108, Lys-109, Lys-118, Arg-119, Trp-122, Lys-149, Lys-152, Lys-155, Ile-156, Leu-158, and Lys-163 have effects on Vps60(128–186) binding, confirming the energetic importance of all of these residues. Consistent with the large buried interface area of the Vta1-Vps60 complex, no single-site mutations could eliminate all detectable Vps60(128–186) binding.

TABLE 2
Binding affinities of Vps60(128–186) for wild-type and mutant Vta1NTD determined by isothermal titration calorimetry assay

Vta1NTD	K_d
	μM
WT	0.7 ± 0.1
K88A	1.2 ± 0.3
I91A	0.9 ± 0.2
M98A	0.9 ± 0.2
L105A	3.1 ± 0.5
K106D	1.1 ± 0.2
L108A	1.4 ± 0.1
K109D	0.8 ± 0.1
K118D	1.7 ± 0.1
R119D	1.05 ± 0.04
W122A	1.4 ± 0.3
W122D	4.7 ± 0.3
K149A	1.0 ± 0.2
K149D	1.9 ± 0.1
K152A	3.9 ± 0.4
K155A	2.3 ± 0.1
I156A	1.5 ± 0.2
L158A	1.5 ± 0.1
K163A	1.1 ± 0.3

Based on the sequence alignment (Fig. 4, *A* and *C*), the Vta1NTD MIT2 domain derived from *S. cerevisiae* has low sequence similarity to the other organisms, whereas

Vps60(128–186) is highly conserved. The highly conserved Vta1NTD MIT2 domain residues Trp-122, Lys-152, and Ile-156 play more important roles in the Vta1-Vps60 interactions. Compared with the wild type, the binding affinities of the W122A, W122D, K152A, and I156A mutants for Vps60(128–186) are reduced by ~2.0-, 6.7-, 5.6-, and 2.1-fold, respectively. Most notably, the non-conserved hydrophobic residues Leu-105 and Leu-108 in helix α5 of Vta1NTD are important as well; the L105A and L108A variants display an ~4.4- to 2.0-fold reduction in the binding affinities for Vps60(128–186). This demonstrates that Vps60(128–186) helix α5′ binds in a more conserved surface groove of Vta1NTD compared with Vps60(128–186) helix α4′ (Fig. 4*A*), indicating that the interactions between Vps60(128–186) helix α5′ and Vta1NTD are more common in all organisms, whereas the interactions between Vps60(128–186) helix α4′ and Vta1NTD make the interactions between Vta1NTD and Vps60(128–186) in yeast unique from those in other organisms. Thus, the Vta1NTD-Vps60(128–186) complex structure provides a structural basis for a previous study that showed that LIP5 (Vta1 in yeast) bound efficiently to a fragment of CHMP5 (Vps60 in yeast) that contained α5 but not α4 (44).

DISCUSSION

Novel Mode of MIT-MIM Interaction—The MIT domain is a versatile protein-protein interaction domain identified in proteins that have a role in vesicle trafficking, including Vps4, Vta1, AMSH, and UBPY, where they mediate interaction within the ESCRT-III complex (45). The MIT domain recognizes sequence motifs called the MIMs primarily within the ESCRT-III subunits. It has been suggested that the interaction between the MIT domain and MIM acts in regulating the disassembly of ESCRT-III, as well as in targeting specific proteins to the site of ESCRT function. At least four types of MIM (MIM1, MIM2, MIM3, and MIM4) were reported to bind to different sites on the MIT domain (Fig. 1) (19–24).

MIM1 contains a sequence-conserved amphipathic helix ((D/E)*xx*L*xx*RL*xx*L(K/R)) along the groove between MIT domain helices α2 and α3 observed in the Vps4-Vps2(183–232) (19) and Vps4-CHMP1A(180–196) (20) complexes. MIM2 is a proline-rich sequence (L^{170}P(E/D)VP^{174} and R^{183}*x*L*x*P*x*LP*x*-PP^{193}) along the groove between MIT domain helices α1 and α3 found in the Vps4-CHMP6(168–179) (21) and Saci1372-Saci1337(183–193) (22) complexes, respectively. MIM3 is a highly specific mode along the groove between MIT domain helices α1 and α3 found in the spastin MIT-CHMP1B(148–196) complex (23) but with an interface twice large as that of the MIT domain of the Vps4-CHMP complex. MIM4 is a mainly polar sequence (E^{203}*xxx*E*xx*ϕ*xx*ϕ*xx*RL*x*TLR^{221}) along a groove made up of helices 3 (Vps4 MIT domain helix 2) and 4/5 (Vps4 MIT domain helix 3) indentified in the AMSHΔC-CHMP3ΔN complex (24). Although the MIM4-binding site resembles the MIM1-binding surface, the contacts between the AMSH MIT domain and MIM4 are mostly polar interactions, whereas hydrophobic interactions play an important role in the Vps4 MIT-MIM1 and Vps4 MIT-MIM2 complexes.

Vta1NTD contains two tandem MIT domains as identified in its crystal structure (29), which mediate the interaction between Vta1 and the ESCRT-III-related proteins Vps60 and Did2. Our NMR structure of Vta1NTD-Vps60(128–186) shows that Vps60 MIM binds exclusively to the second MIT domain of Vta1. Unlike other MIMs, the Vps60 MIM sequence (residues 140–186, defined as MIM5) is much longer and forms two helices (α4′ and α5′). The significant difference from the other MIMs is that Vps60 MIM5 can bind both surfaces made up of helices 5 and 7 (Vps4 MIT domain helices 1 and 3) and helices 6 and 7 (Vps4 MIT domain helices 2 and 3) of the Vta1 MIT2 domain. The Vta1 MIT2-Vps60 MIM5 contacts are a mixture of polar and hydrophobic interactions, as is the case for spastin MIT-MIM3. Thus, the structure of the Vta1-Vps60 complex provides a novel recognition mode of the MIT domain with its ligand and extends the diversity of MIT domain interaction surfaces for peptide ligands.

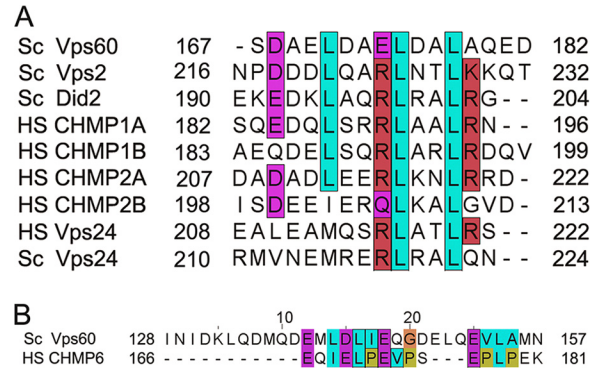

FIGURE 5. **Sequence alignments of Vps60(128–186) helices α4′ and α5′ with conserved MIM1 and MIM2.** *A*, Vps60(128–186) helix α5′ with MIM1 sequences. *B*, Vps60(128–186) helix α4′ with MIM2 sequences. *Sc*, *S. cerevisiae*; *HS*, *Homo sapiens*.

Vps60 Enhances Vta1 Stimulation of Vps4 in a Complex Manner—The dynamic assembly and disassembly of the ESCRT-III polymer play a critical role in ESCRT-mediated membrane deformation events and alterations of Vps4 ATPase activity. To address how Vps60 and Did2 binding enhances Vta1 stimulation of Vps4 ATPase activity, two models were presented (27). One is that their binding to the MIT2 domain results in conformation changes in Vta1; the other is that the interaction between Vta1 and Did2 or Vps60 increases the local concentration of Vta1-Vps4 *in vitro*. It was reported that removal of the two Vta1 tandem MIT domains (Vta1(165–330)) does not enhance the basal activation of Vps4 by Vta1, implying that Vta1 MIT domains do not autoinhibit Vps4 activation (27). The current NMR structure of the Vta1NTD-Vps60(128–186) complex provides further evidence that Vps60 binding does not induce overall conformational changes in the N terminus of Vta1 (Fig. 2*F*) and thus might not lead to further structural arrangement in the C-terminal domain of Vta1. These observations suggest that Vps60 may not allosterically regulate Vta1 and thus could not potentiate its ability to activate Vps4.

The residues within Vps60(128–186) helix α5′ in the interface are composed of the sequence $D^{168'}$*xx*$L^{171'}$*xx*($E^{174'}$)-$L^{175'}$*xx*$L^{178'}$($A^{179'}$) (Fig. 5*A*), nearly identical to CHMP1A-(180–196) MIM1 ((D/E)*xx*L*xx*RL*xx*L(K/R)) (19, 20), except for Glu-174′ and Ala-179′ in contrast to the positively charged residues Arg-190 and Arg-195 in CHMP1A(180–196). In

the Vta1NTD-Vps60(128–186) structure, the Vta1NTD MIT2 domain recognizes a new residue sequence ($L^{143'}(I^{144'})xxxxE^{149'}L^{150'}xE^{152'}V^{153'}L^{154'}$) within Vps60(128–186) helix $\alpha4'$, which has low sequence similarity to CHMP6 MIM2 (Fig. 5*B*) (21), although Leu-143′, Glu-145′, Glu-152′, and Leu-154′ are conserved. Therefore, the interactions between Vta1 and Vps60 implied by the current complex structure do not mimic the interactions between Vps4 and the ESCRT-III subunits CHMP1A(180–196) and CHMP6(168–179). Thus, it is plausible that the specific interaction between Vta1 and Vps60 increases the local concentration of Vta1-Vps4 *in vitro* to enhance Vta1-Vps4 binding and thereby stimulate Vps4 activity.

Taken together, the complex structure of Vta1NTD-Vps60(128–186) cannot account for all aspects of Vps4 activation, but it demonstrates a novel MIT recognition mode that has not been reported. Thus, to address how Vps4 ATPase is activated, further studies of the dynamics of ESCRT-III assembly and disassembly will be performed to better understand the precise function of Vta1 in the process of MVB sorting. The current structure further confirms that the interaction between Vps60 and Vta1 stimulates Vps4 ATPase in an unexpected manner.

REFERENCES

1. Gruenberg, J., and Stenmark, H. (2004) The biogenesis of multivesicular endosomes. *Nat. Rev. Mol. Cell Biol.* **5,** 317–323
2. Morita, E., and Sundquist, W. I. (2004) Retrovirus budding. *Annu. Rev. Cell Dev. Biol.* **20,** 395–425
3. Carlton, J. G., and Martin-Serrano, J. (2007) Parallels between cytokinesis and retroviral budding: a role for the ESCRT machinery. *Science* **316,** 1908–1912
4. Babst, M. (2005) A protein's final ESCRT. *Traffic* **6,** 2–9
5. Hurley, J. H., and Emr, S. D. (2006) The ESCRT complexes: structure and mechanism of a membrane-trafficking network. *Annu. Rev. Biophys. Biomol. Struct.* **35,** 277–298
6. Piper, R. C., and Katzmann, D. J. (2007) Biogenesis and function of multivesicular bodies. *Annu. Rev. Cell Dev. Biol.* **23,** 519–547
7. Winter, V., and Hauser, M. T. (2006) Exploring the ESCRTing machinery in eukaryotes. *Trends Plant Sci.* **11,** 115–123
8. Katzmann, D. J., Odorizzi, G., and Emr, S. D. (2002) Receptor down-regulation and multivesicular-body sorting. *Nat. Rev. Mol. Cell Biol.* **3,** 893–905
9. Saksena, S., and Emr, S. D. (2009) ESCRTs and human disease. *Biochem. Soc. Trans.* **37,** 167–172
10. Raiborg, C., and Stenmark, H. (2009) The ESCRT machinery in endosomal sorting of ubiquitylated membrane proteins. *Nature* **458,** 445–452
11. Bieniasz, P. D. (2009) The cell biology of HIV-1 virion genesis. *Cell Host Microbe* **5,** 550–558
12. Fujii, K., Hurley, J. H., and Freed, E. O. (2007) Beyond Tsg101: the role of Alix in 'ESCRTing' HIV-1. *Nat. Rev. Microbiol.* **5,** 912–916
13. Williams, R. L., and Urbé, S. (2007) The emerging shape of the ESCRT machinery. *Nat. Rev. Mol. Cell Biol.* **8,** 355–368
14. Hurley, J. H. (2008) ESCRT complexes and the biogenesis of multivesicular bodies. *Curr. Opin. Cell Biol.* **20,** 4–11
15. Babst, M., Wendland, B., Estepa, E. J., and Emr, S. D. (1998) The Vps4p AAA ATPase regulates membrane association of a Vps protein complex required for normal endosome function. *EMBO J.* **17,** 2982–2993
16. Xiao, J., Xia, H., Yoshino-Koh, K., Zhou, J., and Xu, Z. (2007) Structural characterization of the ATPase reaction cycle of endosomal AAA protein Vps4. *J. Mol. Biol.* **374,** 655–670
17. Yu, Z., Gonciarz, M. D., Sundquist, W. I., Hill, C. P., and Jensen, G. J. (2008) Cryo-EM structure of dodecameric Vps4p and its 2:1 complex with Vta1p. *J. Mol. Biol.* **377,** 364–377
18. Shestakova, A., Hanono, A., Drosner, S., Curtiss, M., Davies, B. A., Katzmann, D. J., and Babst, M. (2010) Assembly of the AAA ATPase Vps4 on ESCRT-III. *Mol. Biol. Cell* **21,** 1059–1071
19. Obita, T., Saksena, S., Ghazi-Tabatabai, S., Gill, D. J., Perisic, O., Emr, S. D., and Williams, R. L. (2007) Structural basis for selective recognition of ESCRT-III by the AAA ATPase Vps4. *Nature* **449,** 735–739
20. Stuchell-Brereton, M. D., Skalicky, J. J., Kieffer, C., Karren, M. A., Ghaffarian, S., and Sundquist, W. I. (2007) ESCRT-III recognition by VPS4 ATPases. *Nature* **449,** 740–744
21. Kieffer, C., Skalicky, J. J., Morita, E., De Domenico, I., Ward, D. M., Kaplan, J., and Sundquist, W. I. (2008) Two distinct modes of ESCRT-III recognition are required for VPS4 functions in lysosomal protein targeting and HIV-1 budding. *Dev. Cell* **15,** 62–73
22. Samson, R. Y., Obita, T., Freund, S. M., Williams, R. L., and Bell, S. D. (2008) A role for the ESCRT system in cell division in archaea. *Science* **322,** 1710–1713
23. Yang, D., Rismanchi, N., Renvoisé, B., Lippincott-Schwartz, J., Blackstone, C., and Hurley, J. H. (2008) Structural basis for midbody targeting of spastin by the ESCRT-III protein CHMP1B. *Nat. Struct. Mol. Biol.* **15,** 1278–1286
24. Solomons, J., Sabin, C., Poudevigne, E., Usami, Y., Hulsik, D. L., Macheboeuf, P., Hartlieb, B., Göttlinger, H., and Weissenhorn, W. (2011) Structural basis for ESCRT-III CHMP3 recruitment of AMSH. *Structure* **19,** 1149–1159
25. Babst, M., Davies, B. A., and Katzmann, D. J. (2011) Regulation of Vps4 during MVB sorting and cytokinesis. *Traffic* **12,** 1298–1305
26. Azmi, I., Davies, B., Dimaano, C., Payne, J., Eckert, D., Babst, M., and Katzmann, D. J. (2006) Recycling of ESCRTs by the AAA-ATPase Vps4 is regulated by a conserved VSL region in Vta1. *J. Cell Biol.* **172,** 705–717
27. Azmi, I. F., Davies, B. A., Xiao, J., Babst, M., Xu, Z., and Katzmann, D. J. (2008) ESCRT-III family members stimulate Vps4 ATPase activity directly or via Vta1. *Dev. Cell* **14,** 50–61
28. Dimaano, C., Jones, C. B., Hanono, A., Curtiss, M., and Babst, M. (2008) Ist1 regulates Vps4 localization and assembly. *Mol. Biol. Cell* **19,** 465–474
29. Xiao, J., Xia, H., Zhou, J., Azmi, I. F., Davies, B. A., Katzmann, D. J., and Xu, Z. (2008) Structural basis of Vta1 function in the multivesicular body sorting pathway. *Dev. Cell* **14,** 37–49
30. Lottridge, J. M., Flannery, A. R., Vincelli, J. L., and Stevens, T. H. (2006) Vta1p and Vps46p regulate the membrane association and ATPase activity of Vps4p at the yeast multivesicular body. *Proc. Natl. Acad. Sci. U.S.A.* **103,** 6202–6207
31. Scott, A., Chung, H. Y., Gonciarz-Swiatek, M., Hill, G. C., Whitby, F. G., Gaspar, J., Holton, J. M., Viswanathan, R., Ghaffarian, S., Hill, C. P., and Sundquist, W. I. (2005) Structural and mechanistic studies of VPS4 proteins. *EMBO J.* **24,** 3658–3669
32. Yang, D., and Hurley, J. H. (2010) Structural role of the Vps4-Vta1 interface in ESCRT-III recycling. *Structure* **18,** 976–984
33. Bax, A., and Grzesiek, S. (1993) Methodological advances in protein NMR. *Acc. Chem. Res.* **26,** 131–138
34. Clore, G. M., and Gronenborn, A. M. (1998) Determining the structures of large proteins and protein complexes by NMR. *Trends Biotechnol.* **16,** 22–34
35. Yamazaki, T., Formankay, J. D., and Kay, L. E. (1993) Two-dimensional NMR experiments for correlating C-13-beta and proton-delta/epsilon chemical shifts of aromatic residues in ^{13}C-labeled proteins via scalar couplings. *J. Am. Chem. Soc.* **115,** 11054–11055
36. Delaglio, F., Grzesiek, S., Vuister, G. W., Zhu, G., Pfeifer, J., and Bax, A. (1995) NMRPipe: a multidimensional spectral processing system based on UNIX pipes. *J. Biomol. NMR* **6,** 277–293
37. Goddard, T. D., and Kneller, D. G. (2001) *SPARKY 3*, University of California, San Francisco
38. Cornilescu, G., Delaglio, F., and Bax, A. (1999) Protein backbone angle restraints from searching a database for chemical shift and sequence homology. *J. Biomol. NMR* **13,** 289–302
39. Wang, C., Shen, J., Yang, Z., Chen, P., Zhao, B., Hu, W., Lan, W., Tong, X., Wu, H., Li, G., and Cao, C. (2011) Structural basis for site-specific reading

of unmodified R2 of histone H3 tail by UHRF1 PHD finger. *Cell Res.* **21,** 1379–1382
40. Laskowski, R. A., Rullmannn, J. A., MacArthur, M. W., Kaptein, R., and Thornton, J. M. (1996) AQUA and PROCHECK-NMR: programs for checking the quality of protein structures solved by NMR. *J. Biomol. NMR* **8,** 477–486
41. Koradi, R., Billeter, M., and Wüthrich, K. (1996) MOLMOL: a program for display and analysis of macromolecular structures. *J. Mol. Graph* **14,** 51–55
42. Muzioł, T., Pineda-Molina, E., Ravelli, R. B., Zamborlini, A., Usami, Y., Göttlinger, H., and Weissenhorn, W. (2006) Structural basis for budding by the ESCRT-III factor CHMP3. *Dev. Cell* **10,** 821–830
43. Wishart, D. S., and Sykes, B. D. (1994) The ^{13}C chemical-shift index: a simple method for the identification of protein secondary structure using ^{13}C chemical-shift data. *J. Biomol. NMR* **4,** 171–180
44. Shim, S., Merrill, S. A., and Hanson, P. I. (2008) Novel interactions of ESCRT-III with LIP5 and VPS4 and their implications for ESCRT-III disassembly. *Mol. Biol. Cell* **19,** 2661–2672
45. Hurley, J. H., and Yang, D. (2008) MIT domainia. *Dev. Cell* **14,** 6–8